Molecular Bases of Disease:

Nod-like Receptor Protein 3 (NLRP3) Inflammasome Activation and Podocyte Injury via Thioredoxin-Interacting Protein (TXNIP) during Hyperhomocysteinemia

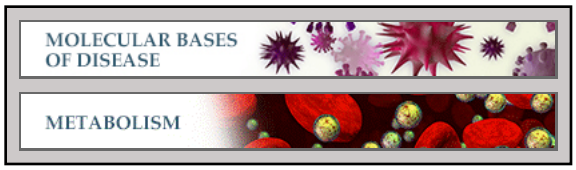

Justine M. Abais, Min Xia, Guangbi Li, Yang Chen, Sabena M. Conley, Todd W. B. Gehr, Krishna M. Boini and Pin-Lan Li

J. Biol. Chem. 2014, 289:27159-27168.
doi: 10.1074/jbc.M114.567537 originally published online August 19, 2014

THE JOURNAL OF BIOLOGICAL CHEMISTRY VOL. 289, NO. 39, pp. 27159–27168, September 26, 2014

Nod-like Receptor Protein 3 (NLRP3) Inflammasome Activation and Podocyte Injury via Thioredoxin-Interacting Protein (TXNIP) during Hyperhomocysteinemia*

Received for publication, March 24, 2014, and in revised form, August 5, 2014 Published, JBC Papers in Press, August 19, 2014, DOI 10.1074/jbc.M114.567537

Justine M. Abais[‡1] Min Xia[‡], Guangbi Li[‡], Yang Chen[‡], Sabena M. Conley[‡], Todd W. B. Gehr[§], Krishna M. Boini[‡], and Pin-Lan Li[‡]

From the Departments of [‡]Pharmacology and Toxicology and [§]Internal Medicine Virginia Commonwealth University, School of Medicine, Richmond, Virginia 23298

Background: Hyperhomocysteinemia (hHcys) contributes to glomerular injury by activating NLRP3 inflammasomes in response to increased oxidative stress.
Results: Thioredoxin-interacting protein (TXNIP) aggregated with NLRP3 inflammasomes, and blocking TXNIP prevented inflammasome activation during hHcys.
Conclusion: TXNIP uniquely links changes in oxidative stress to hHcys-induced NLRP3 inflammasome activation.
Significance: Glomerular injury related to hHcys can be prevented by TXNIP inhibition.

NADPH oxidase-derived reactive oxygen species (ROS) have been reported to activate NLRP3 inflammasomes resulting in podocyte and glomerular injury during hyperhomocysteinemia (hHcys). However, the mechanism by which the inflammasome senses ROS is still unknown in podocytes upon hHcys stimulation. The current study explored whether thioredoxin-interacting protein (TXNIP), an endogenous inhibitor of the antioxidant thioredoxin and ROS sensor, mediates hHcys-induced NLRP3 inflammasome activation and consequent glomerular injury. In cultured podocytes, size exclusion chromatography and confocal microscopy showed that inhibition of TXNIP by siRNA or verapamil prevented Hcys-induced TXNIP protein recruitment to form NLRP3 inflammasomes and abolished Hcys-induced increases in caspase-1 activity and IL-1β production. TXNIP inhibition protected podocytes from injury as shown by normal expression levels of podocyte markers, podocin and desmin. *In vivo*, adult C57BL/6J male mice were fed a folate-free diet for 4 weeks to induce hHcys, and TXNIP was inhibited by verapamil (1 mg/ml in drinking water) or by local microbubble-ultrasound TXNIP shRNA transfection. Evidenced by immunofluorescence and co-immunoprecipitation studies, glomerular inflammasome formation and TXNIP binding to NLRP3 were markedly increased in mice with hHcys but not in TXNIP shRNA-transfected mice or those receiving verapamil. Furthermore, TXNIP inhibition significantly reduced caspase-1 activity and IL-1β production in glomeruli of mice with hHcys. Correspondingly, TXNIP shRNA transfection and verapamil attenuated hHcys-induced proteinuria, albuminuria, glomerular damage, and podocyte injury. In conclusion, our results demonstrate that TXNIP binding to NLRP3 is a key signaling mechanism necessary for hHcys-induced NLRP3 inflammasome formation and activation and subsequent glomerular injury.

The Nod-like receptor protein 3 (NLRP3)[2] inflammasome, found to be a key mediator of the innate immune system in response to a host of initiating factors, has been extensively demonstrated to be activated in response to a wide range of danger signals derived from disease and infection (1–5). The formation of this novel cytosolic multiprotein complex requires the oligomerization of the three inflammasome components: NLRP3 protein, the adaptor molecule apoptosis-associated speck-like protein containing a CARD (caspase recruitment domain) (ASC), and the cysteine protease caspase-1, which causes the maturation of proinflammatory cytokines IL-1β and IL-18. It is assumed that this inflammasome activation and extracellular secretion of inflammatory cytokines sense diverse danger signals and instigate the innate inflammatory response (6). More recently, NLRP3 inflammasome activation has been reported to trigger many other cell injury responses far beyond inflammation (7).

Elevated levels of homocysteine (Hcys), a methionine-derived essential amino acid, are associated with a number of pathologies, including cardiovascular and renal diseases, neurocognitive diseases, and accelerating the aging process in general (8–10). Hyperhomocysteinemia (hHcys) is regarded as an important independent risk factor in the development of end stage renal disease, and our recent studies have shown that activation of NLRP3 inflammasomes contributes to the development of hHcys-induced glomerular injury and podocyte injury in mice (11). This hHcys-induced NLRP3 inflammasome activating process was shown to depend on NADPH oxidase and the reactive oxygen species (ROS) derived from its activation, specifically superoxide (O_2^-) and hydrogen peroxide

* This work was supported, in whole or in part, by Grants DK54927, HL075316, and HL57244 (to P.-L. L.) and 1F31AG043289-01 (to J. M. A.) from the National Institutes of Health.
[1] To whom correspondence should be addressed: Dept. of Pharmacology and Toxicology, Virginia Commonwealth University, School of Medicine, 410 N. 12th St., Richmond, VA 23298. Tel.: 804-828-4793; Fax: 804-828-4794; E-mail: pli@vcu.edu.

[2] The abbreviations used are: NLRP3, Nod-like receptor protein 3; FF, folate-free; hHcys, hyperhomocysteinemia; Hcys, homocysteine; ND, normal diet; SEC, size-exclusion chromatography; ER, endoplasmic reticulum.

(H_2O_2), where inhibition of the gp91^{phox} subunit of NADPH oxidase or scavenging of O_2^- and H_2O_2 suppressed NLRP3 inflammasome activation and furthermore ameliorated subsequent glomerular dysfunction (12, 13). However, the exact mechanism of how this NADPH oxidase-derived ROS is sensed by podocytes to form the NLRP3 inflammasome and thereby lead to its activation in glomerular podocyte cells is still largely unknown. In this regard, the canonical work done by Zhou *et al.* (14) provided strong evidence of thioredoxin-interacting protein (TXNIP) as a binding partner to NLRP3, where association between these two proteins was necessary for downstream inflammasome activation. TXNIP, the negative regulator of the antioxidant thioredoxin, may time-dependently dissociate from thioredoxin to bind with NLRP3 leading to inflammasome formation and activation.

The present study was designed to investigate the role of TXNIP during hHcys and to explore its potential effects on NLRP3 inflammasome activation and consequent podocyte injury and glomerular sclerosis. We first characterized the feature of TXNIP binding to NLRP3 and its related role in the formation and activation of NLRP3 inflammasomes using cultured podocytes. Then, we determined the pathological role of TXNIP-mediated activation of NLRP3 inflammasomes in mice with hHcys. These studies together elucidate the key role of TXNIP in bridging redox signals with activation of NLRP3 inflammasomes, leading to podocyte injury and ultimate glomerular sclerosis.

EXPERIMENTAL PROCEDURES

Podocyte Culture—Graciously provided by Dr. Paul E. Klotman (Division of Nephrology, Department of Medicine, Mount Sinai School of Medicine, New York, NY), a conditionally immortalized mouse podocyte cell line was cultured undifferentiated in the presence of 10 units/ml recombinant mouse interferon-γ at 33 °C on collagen I-coated flasks in serum-containing RPMI 1640 medium (15). Readers are directed to the following reference for complete detail regarding the generation of this cell line (16). Podocytes were used for experiments after differentiation at 37 °C for 10–14 days in the absence of interferon-γ. L-Hcys (40 μM), verapamil (50 μM), and tunicamycin (1 μg/ml), doses selected based on dose-dependent studies, were added separately or together to cultured podocytes for 24 h (11). Podocytes that were transfected with TXNIP siRNA (Invitrogen) were incubated with a serum-free medium for 15 min prior to TXNIP siRNA transfection using the siLentFect Lipid Reagent (Bio-Rad) according to the manufacturer's instructions. After 18 h of incubation with the siRNA at 37 °C, the medium was changed, and cells were treated with 40 μM Hcys for 24 h.

Animals and Gene Transfection by Ultrasound Microbubble—Eight-week-old male C57BL/6J mice (The Jackson Laboratory, Bar Harbor, ME) were used in this study. As an accepted method of accelerating renal injury, mice were uninephrectomized (17, 18). After allowing 1 week for surgery recovery, a preparation of plasmid encoding for either TXNIP short hairpin RNA (shRNA) or the reporter gene luciferase was mixed with cationically charged Optison microbubbles (GE Healthcare) and then injected into the femoral artery and locally transfected to the kidney by sonoporation. Another group of mice received verapamil in the drinking water (1 mg/ml), equating to a dose of ~100 mg/kg/day (19). For 4 weeks, mice were maintained on either a normal diet (ND) or a folate-free (FF) diet (Dyets, Inc., Bethlehem, PA) to induce hHcys. At the end of the 4-week treatment, mice were placed in metabolic cages for 24 h to collect urine samples. Following metabolic cages, blood and plasma was collected, mice were sacrificed, and kidney tissue was harvested for experimental analysis. The Institutional Animal Care and Use Committee of Virginia Commonwealth University approved all animal procedures and protocols used in this study.

Size-exclusion Chromatography (SEC)—As described in our previous studies (12, 13), homogenate from treated podocytes was prepared using SEC protein extraction buffer: 20 mM 4-(2-hydroxyethyl)-1-piperazineethanesulfonic acid-KOH (pH 7.5), 10 mM KCl, 1.5 mM Na-EDTA, 1 mM Na-EGTA, and 1× protease inhibitor mixture (Roche Applied Science). Samples were centrifuged at maximum speed for 10 min at 4 °C, and the supernatant was filtered through a 0.45-μm centrifuge tube filter and normalized by measuring the protein concentration. Samples were normalized by loading 1 mg of protein in a <500-μl total volume onto a Superose 6 10/300 GL column using an ÄKTAprime plus fast-protein liquid chromatography (FPLC) system (GE Healthcare). Fractions were collected (600 μl), and protein was precipitated using trichloroacetic acid and analyzed by SDS-PAGE electrophoresis. Samples were run on a 12% gel, transferring protein at 100 V for 1 h, blocking with 5% nonfat dry milk in Tris-buffered saline with 0.1% Tween 20 for 1 h, and using a rabbit anti-NLRP3 (1:500, Abcam, Cambridge, MA) or mouse anti-TXNIP (1:1000, MBL International, Woburn, MA) antibody overnight at 4 °C. Next, membranes were incubated with the appropriate horseradish peroxidase-labeled IgG (1:5000) at room temperature for 1 h, and the chemiluminescent bands were exposed with Kodak Omat x-ray film, using ImageJ software (National Institutes of Health, Bethesda, MD) to quantify band density.

Indirect Immunofluorescent Confocal Microscopy—Indirect immunofluorescent staining was used to observe the colocalization of inflammasome and podocyte marker proteins in both cultured cells as well as frozen mouse kidney sections, with the method described previously in detail (12, 13). Briefly, podocytes seeded in eight-well chambers were fixed, washed, and blocked before being incubated in primary antibodies (1:100) overnight at 4 °C. The primary antibodies used were as follows: goat anti-NLRP3 (Abcam, Cambridge, MA) with rabbit anti-ASC (Santa Cruz Biotechnology, Dallas, TX), or goat anti-NLRP3 with mouse anti-TXNIP (MBL International). Frozen mouse kidney sections were also fixed in acetone, blocked, then incubated with the same aforementioned primary antibodies (1:50) overnight at 4 °C. Some coverslips with podocytes and frozen kidney sections were only stained for podocyte markers podocin (1:50; Sigma) or desmin (1:50; BD Biosciences). Double immunofluorescent staining was performed by Alexa Fluor 488 or Alexa Fluor 555-labeled secondary antibody (1:200 podocytes, 1:50 frozen kidney slides; Invitrogen) incubation for 1 h at room temperature. Slides were then washed, mounted, and observed using a confocal laser scanning microscope (Fluoview

FV1000, Olympus, Japan) and Image Pro Plus software (version 6.0; Media Cybernetics, Bethesda, MD) was used to analyze colocalization, which was expressed as the Pearson correlation coefficient.

Caspase-1 Activity and IL-1β and VEGF Measurements—Caspase-1 activity was measured by a commercially available colorimetric assay (Biovision, Mountain View, CA), whereas IL-1β production and vascular endothelial growth factor (VEGF)-A secretion was measured in the supernatant of cultured podocytes using an enzyme-linked immunosorbent assay (R&D Systems, Minneapolis, MN) according to the manufacturer's instructions.

In Vivo Imaging and Monitoring of Gene Expression—To monitor the efficiency of gene expression through somatic plasmid transfection daily, anesthetized mice were injected with an aqueous solution of luciferin (150 mg/kg intraperitoneal) before being imaged using the Xenogen IVIS200 *in vivo* imaging system (PerkinElmer Life Sciences) as described in detail previously (11).

Real-time Reverse Transcription-Polymerase Chain Reaction (RT-PCR)—Total RNA was isolated from renal cortical tissue, reverse transcribed to cDNA, and subjected to PCR amplification according to the procedures described previously (20). TXNIP primers were synthesized by Operon (Huntsville, AL) with the following sense (CAGCCTACAGCAGGTGAGAAC) and antisense (CTCATCTCAGAGCTCGTCCG) sequence.

Co-immunoprecipitation—Renal cortical tissue was homogenized on ice in immunoprecipitation lysis buffer (30 mM Tris-HCl, 150 mM NaCl, 2 mM EDTA, 1% Triton X-100, 10% glycerol, 1× protease inhibitor) followed by brief pulses of hand sonication. After a 30-min incubation on ice, the lysate was centrifuged, and the supernatant precleared by incubation with Protein A/G PLUS-agarose beads (Santa Cruz Biotechnology, sc-2003) in 4 °C. The precleared supernatant was incubated with 2 μg of antibody against NLRP3 (Abcam) for 4 h on a rocker in 4 °C. Beads were added for an additional 1 h, and then immunoprecipitates were collected by centrifugation at 1,000 × *g* for 5 min and washed three times with immunoprecipitation lysis buffer with centrifugation after each wash. The pellet was resuspended in 2× sample buffer, boiled, and analyzed for NLRP3 and TXNIP protein expression by Western blot, as described above.

Urinary Protein and Albumin Measurements—Total urinary protein excretion was determined spectrophotometrically using the Bradford assay (Sigma), and urinary albumin excretion was measured using a commercially available mouse albumin ELISA kit (Bethyl Laboratories, Montgomery, TX).

Glomerular Morphological Examinations—Fixed kidney tissues were paraffin-embedded, sectioned, and stained with periodic acid-Schiff. Using a light microscope, glomerular morphology was observed and assessed semiquantitatively as described in detail previously (13, 21).

Intracellular $[Ca^{2+}]_i$ Measurement—Intracellular Ca^{2+} response to Hcys and verapamil was determined by using the Ca^{2+}-sensitive fluorescent dye, Fura-2, with a fluorescence imaging system as described previously (22–24). Briefly, treated podocytes were loaded with 10 μM Fura-2 at room temperature for 30 min followed by washing three times with Ca^{2+}-free Hanks' buffer supplemented with 2 μM EGTA. The ratio of Fura-2 emissions after excitation at 340 and 380 nm was monitored by using an inverted Nikon Diaphot 200 microscope (Tokyo, Japan) and a SPOT RT Monochrome digital camera (Diagnostic Instruments, Sterling Heights, MI).

Apoptosis Assay—As described in our previous studies, podocyte apoptosis was detected using an annexin V-propidium iodide double staining kit (Sigma) according to the manufacturer's instructions (25).

High-performance Liquid Chromatography Analysis of Plasma Hcys Concentration—Hcys levels in mouse plasma were analyzed by methods described previously in detail (26).

Statistical Analysis—Data are expressed as mean ± S.E., where significance was determined using one-way or two-way analysis of variance followed by the Student-Newman-Keuls post hoc test. χ^2 test was used to determine significance of ratio and percentage data. $p < 0.05$ was considered statistically significant.

RESULTS

TXNIP Inhibition Prevented Recruitment of TXNIP Protein to NLRP3 Inflammasome Fractions—In the chromatogram illustrating a typical standard and sample elution profile, the elution of inflammasome proteins in earlier fractions signifies the aggregation of inflammasome proteins to higher molecular weight complexes and the formation of inflammasomes (Fig. 1*A*). Demonstrated by SEC in previous studies, Hcys stimulation of podocytes resulted in increased NLRP3 inflammasome formation (11, 12). The present study further validated this concept as shown by the increased expression of NLRP3 protein in fractions 4–7, termed the inflammasome fractions in Hcys-treated podocytes (Fig. 1*B*). In these podocytes stimulated by Hcys, we also observed the recruitment of TXNIP to the inflammasome fractions, suggesting TXNIP aggregation to the NLRP3 inflammasome complex. To further elucidate the role of TXNIP, we pretreated Hcys-stimulated podocytes with siRNA or verapamil to inhibit its expression and found that inhibition of TXNIP not only prevented its own shift to the inflammasome fractions but also blocked the formation of NLRP3 complex in podocytes in response to Hcys stimulations. The relative band intensities at fractions 4–7 were quantified and summarized in Fig. 1*C*. These SEC results provided strong evidence for a possible role of TXNIP and its aggregation with the inflammasome complex in Hcys-induced NLRP3 inflammasome formation.

Inhibition of TXNIP Attenuated Hcys-induced TXNIP-NLRP3 Binding and NLRP3 Inflammasome Formation—As an additional method for detection of NLRP3 inflammasome formation, confocal microscopy was used to observe the colocalization of inflammasome proteins in podocytes. As shown in Fig. 2*A* and quantified in Fig. 2, *B* and *C*, Hcys increased the colocalization of NLRP3 (*green*) and ASC (*red*) compared with control cells, suggesting the formation of NLRP3 inflammasomes in podocytes. Furthermore, Hcys stimulation also increased the colocalization of NLRP3 (*green*) with TXNIP (*red*), suggesting that Hcys induces the aggregation of TXNIP together with NLRP3. However, prior treatment with TXNIP siRNA or verapamil significantly attenuated the colocal-

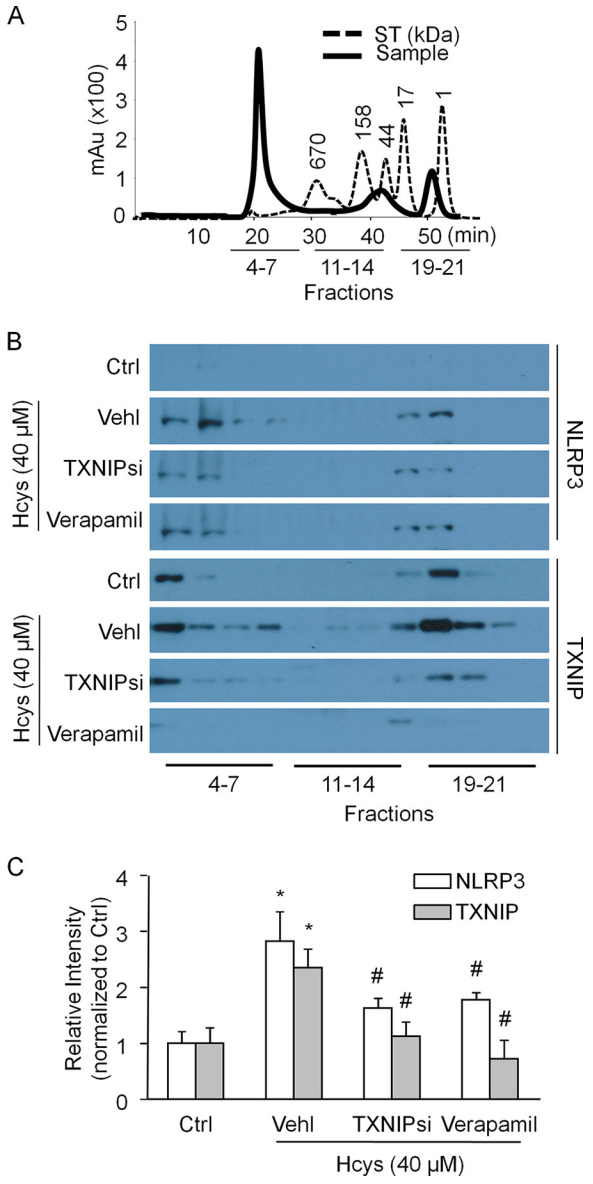

FIGURE 1. **TXNIP and NLRP3 recruitment to the high molecular weight inflammasome fractions upon stimulation with Hcys.** *A*, SEC chromatogram illustrating the elution curves of a typical standard and podocyte protein sample. *B*, representative Western blot gel documents depicting the shift of NLRP3 and TXNIP protein during Hcys treatment, which was prevented during TXNIP inhibition. *C*, summarized quantification of either NLRP3 or TXNIP protein residing in the inflammasome fractions ($n = 4$). *mAu*, milliabsorbance units; *ST*, standard; *Ctrl*, control; *Vehl*, vehicle; *TXNIPsi*, TXNIP siRNA. *, $p < 0.05$ *versus* control; #, $p < 0.05$ *versus* Hcys.

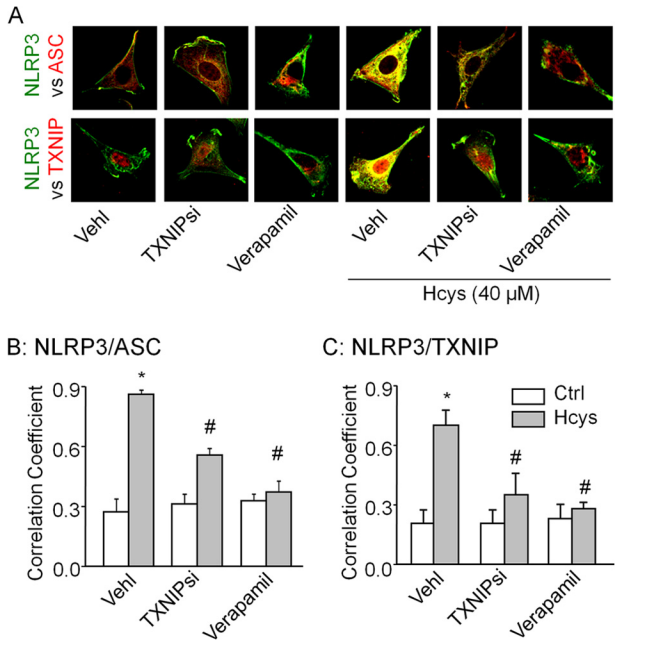

FIGURE 2. **TXNIP inhibition prevented Hcys-induced NLRP3 inflammasome formation.** *A*, confocal microscopic detection of NLRP3 (*green*) with ASC (*red*) and NLRP3 (*green*) with TXNIP (*red*) and their colocalization together (*yellow*), indicative of the inflammasome formation. *B* and *C*, summarized data showing the quantification of the extent of colocalization between NLRP3 with ASC and NLRP3 with TXNIP ($n = 4–6$). *Ctrl*, control; *Vehl*, vehicle; *TXNIPsi*, TXNIP siRNA. *, $p < 0.05$ *versus* vehicle-control; #, $p < 0.05$ *versus* vehicle-Hcys.

ization of NLRP3 with either ASC or TXNIP. This reveals that TXNIP expression and its binding to NLRP3 are necessary for NLRP3 inflammasome formation in Hcys-treated podocytes.

Inhibition of TXNIP Abrogated Hcys-induced Increases in Caspase-1 Activity and IL-1β Secretion—First demonstrated by Srinivasula *et al.* (27), it is known that the formation of NLRP3 inflammasomes results in downstream caspase-1 activation and subsequent IL-1β maturation. These effects reflect the functionality of the formed inflammasomes and thus were used to determine the effect of TXNIP inhibition on Hcys-induced inflammasome activation in the current study. Hcys treatment significantly increased caspase-1 activity and IL-1β production in podocytes compared with control cells, suggesting activation of NLRP3 inflammasomes (Fig. 3, *A* and *B*). Both TXNIP siRNA transfection and pretreatment with verapamil significantly attenuated Hcys-induced caspase-1 activity and IL-1B production. However, endoplasmic reticulum (ER) stress agent tunicamycin was not able to induce NLRP3 inflammasome activation, eliminating the potential contribution of ER-derived oxidative stress (Fig. 3, *C* and *D*). Additionally, measurement of intracellular calcium ($[Ca^{2+}]_i$) determined that the inflammasome-activating effects of Hcys were not attributable to an elevation in $[Ca^{2+}]_i$, and furthermore, the inflammasome-inhibiting effects of verapamil were not due to inhibition of $[Ca^{2+}]_i$ (Fig. 3*E*).

Protection from Hcys-induced Podocyte Damage by TXNIP Inhibition—To assess the extent of podocyte damage, the protein expression of slit diaphragm molecules such as podocin and desmin was monitored. Podocin, a podocyte-specific marker, decreases in expression during injury, whereas podocyte damage marker desmin increases during injury (28, 29). Immunofluorescence analysis demonstrated that Hcys-treated podocytes displayed a dramatic decrease in podocin staining and increase in desmin staining, signifying podocyte damage (Fig. 4*A*). However, TXNIP inhibition resulted in the protection of these podocyte damages as shown by normalized podocin and desmin protein expression to control levels. Quantification of fluorescence was summarized in Figs. 4*B*. Moreover, the ability of podocytes to secrete VEGF is considered to be an additional measure of podocyte functionality (30). Hcys-injured podocytes displayed impaired secretion of VEGF, which was precluded in TXNIP siRNA- or verapamil-treated cells (Fig. 4*C*). Additionally, TXNIP inhibition by verapamil prevented

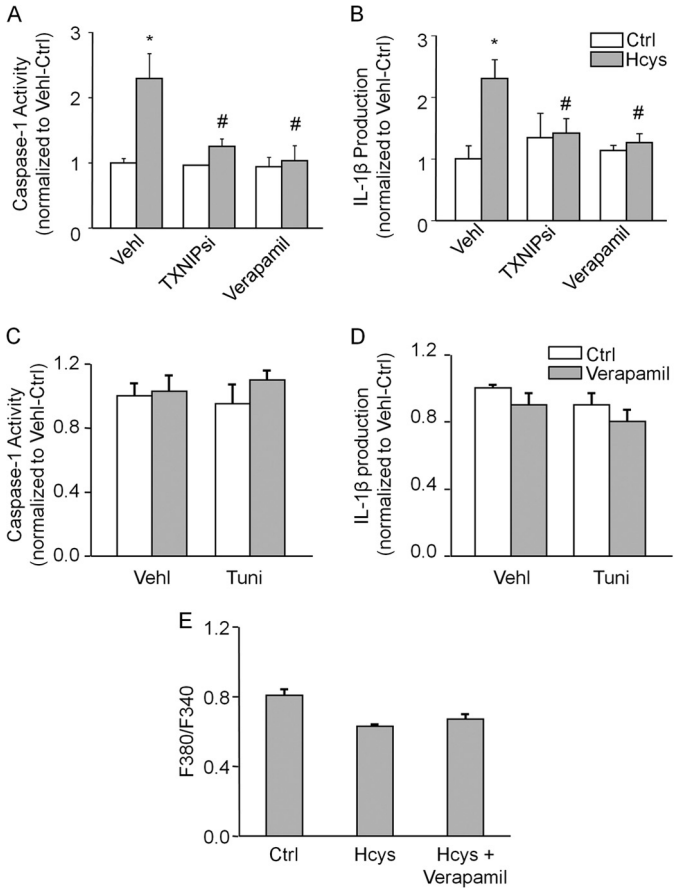

FIGURE 3. **Attenuation of Hcys-induced NLRP3 inflammasome activation by TXNIP blockade.** *A*, effect of TXNIPsi and verapamil on Hcys-induced NLRP3 inflammasome activation, shown as the fold change of caspase-1 activation *versus* vehicle control (*Vehl-Ctrl*) ($n = 7–8$). *B*, measured in the supernatant of cultured podocytes, TXNIP inhibition suppressed Hcys-induced IL-1β production ($n = 8$). *C*, tunicamycin-treated cells displayed no change in caspase-1 activity, indicating no significant effect of ER stress on inflammasome activation in podocytes ($n = 5–6$). *D*, no change in IL-1β production in the supernatant of tunicamycin-treated podocytes validated caspase-1 activation results ($n = 5–6$). *E*, measurement of $[Ca^{2+}]_i$ demonstrated that verapamil inhibition of Hcys-induced NLRP3 inflammasome activation was not due to its calcium channel blocker properties ($n = 4$). *Ctrl*, control; *Vehl*, vehicle; *Tuni*, tunicamycin; *TXNIPsi*, TXNIP siRNA. *, $p < 0.05$ *versus* vehicle control; #, $p < 0.05$ *versus* vehicle Hcys.

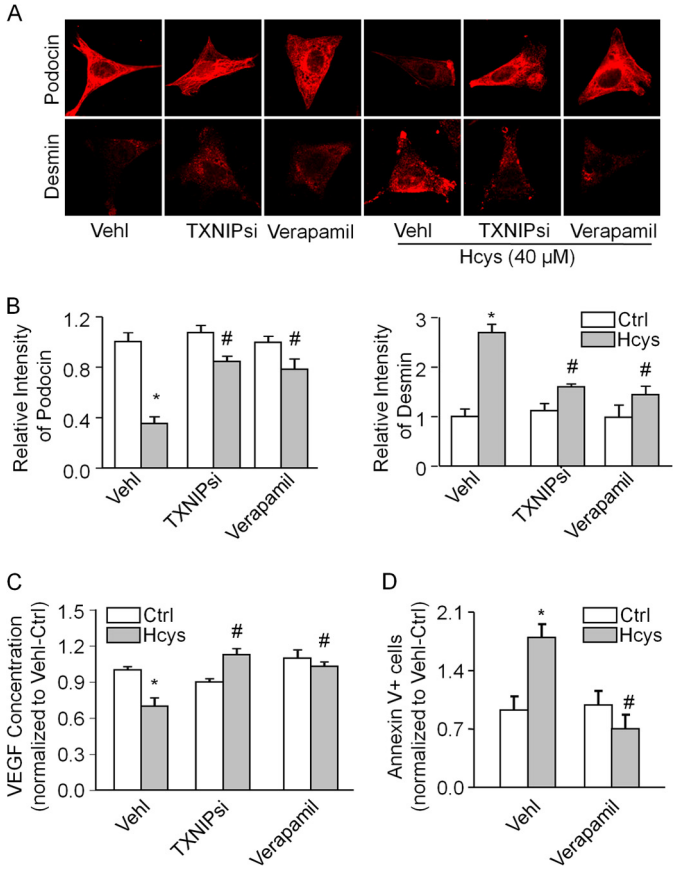

FIGURE 4. **Inhibition of TXNIP preserved podocytes integrity.** *A*, immunofluorescence staining of podocyte-specific marker podocin and podocyte injury marker desmin, where Hcys-induced decrease in podocin and increase in desmin expression were attenuated by TXNIPsi and verapamil. *B*, summarized data showing the relative intensity of podocin and desmin staining ($n = 6$). *C*, VEGF was measured in the supernatant of podocytes and used as an indicator of podocyte functionality, where Hcys-damaged podocytes suppressed VEGF secretion, which was restored upon TXNIP inhibition ($n = 6$). *D*, Hcys treatment increased the population of annexin V^+ podocytes, indicative of increased cell death, which was prevented upon verapamil administration ($n = 6$). *Ctrl*, control; *Vehl*, vehicle; *TXNIPsi*, TXNIP siRNA. *, $p < 0.05$ *versus* vehicle control; #, $p < 0.05$ *versus* vehicle Hcys.

Hcys-induced podocyte cell death (Fig. 4*D*). Together, these data suggest that TXNIP mediates Hcys-induced podocyte dysfunction and that inhibition of TXNIP ameliorates the deleterious effects of Hcys or inflammation activation on podocytes.

Local in Vivo TXNIP shRNA Transfection Inhibited TXNIP mRNA and Protein Expression in Mouse Kidneys—To further determine the role of TXNIP in NLRP3 inflammasome activation and glomerular injury in mice, we transfected TXNIP shRNA locally into the kidney. Our previous reports have demonstrated that introduction of plasmids locally into mouse kidneys by the ultrasound microbubble technique displayed stable expression of transfected gene for at least 4 weeks (31). To monitor plasmid transfection efficiency, a plasmid with a luciferase expression vector was cotransfected together with the targeting TXNIP shRNA plasmid to act as a reporter. Fig. 5*A* represents *in vivo* expression images of kidneys monitored 3, 7, and 14 days post-transfection by a rodent animal *in vivo* imaging system. In a hemidissected kidney 4 days post-transfection, a strong luciferase signal was detected in the renal cortex, where the observed signal represents efficient transfection and gene expression (Fig. 5*B*). It was demonstrated that efficient transfection of plasmids and gene expression were maintained throughout experiments and such *in vivo* imaging of gene expression was used to determine whether mice can continue for further functional studies. After transfected mice were maintained on either a normal or FF diet for 4 weeks, the TXNIP mRNA levels in the kidney were assessed by real time RT-PCR to validate the efficiency of plasmid transfection and gene expression. As shown in Fig. 5*C*, TXNIP shRNA transfection significantly decreased TXNIP mRNA expression in mice on the ND when compared with those transfected only with luciferase plasmids. Although TXNIP mRNA expression increased in luciferase-transfected mice maintained on the FF diet, TXNIP shRNA-transfected mice exhibited substantially reduced TXNIP mRNA expression. These findings translated to the protein level, demonstrated by immunofluorescent staining of TXNIP in the glomeruli of transfected mice (Fig. 5*D*). Together, we concluded that TXNIP shRNA was efficiently

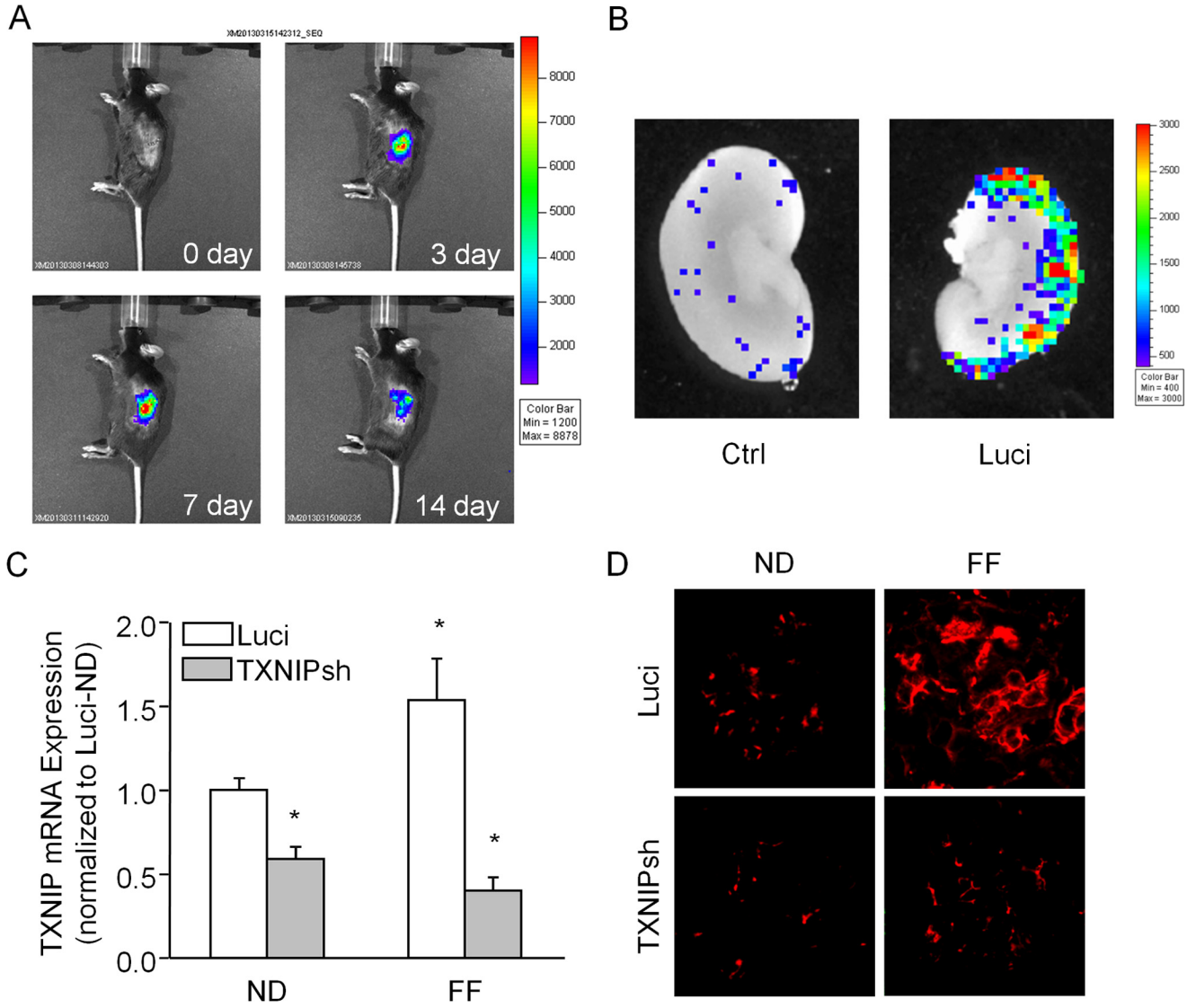

FIGURE 5. **Efficiency of local *in vivo* transfection of TXNIP shRNA into the renal cortex by the ultrasound microbubble technique.** *A*, images taken 3, 7, and 14 days post-transfection by an *in vivo* imaging system daily confirmed transfection efficiency. *B*, *ex vivo* image 4 days after transfection of hemidissected kidney demonstrated successful localized gene expression. *C*, real time RT-PCR data quantifying mRNA silencing efficiency of the plasmid after 4 weeks of maintenance on either a ND or FF diet ($n = 6$). *D*, immunofluorescent staining of TXNIP in the glomeruli of transfected mice. *Luci*, luciferase; *TXNIPsh*, TXNIP shRNA. *, $p < 0.05$ *versus* luciferase-ND.

delivered locally to the mouse kidney and were successfully being expressed, evident by the markedly reduced TXNIP expression in glomeruli of mice.

In Vivo TXNIP Inhibition Prevented hHcys-induced TXNIP-NLRP3 Binding and NLRP3 Inflammasome Formation in Glomeruli—After 4 weeks of uninephrectomized mice receiving the FF diet regiment, mice developed hHcys which resulted in NLRP3 inflammasome formation in their glomeruli, mainly in podocytes as shown in our previous studies (11, 13). Illustrated in Fig. 6*A*, confocal microscopic analysis demonstrated that FF diet-fed mice increased colocalization of NLRP3 with ASC (increased *yellow* staining) in glomeruli of luciferase transfected mice compared with ND fed mice, suggesting glomerular NLRP3 inflammasome formation during hHcys. This was further accompanied with an increase in TXNIP expression, which colocalized significantly with NLRP3, and possible binding to the NLRP3-ASC-caspase-1 inflammasome complex. However, TXNIP inhibition (either by verapamil or TXNIP shRNA transfection) substantially suppressed colocalization of NLRP3 with either ASC or TXNIP (Fig. 6*A*). This colocalization was quantified and summarized in Fig. 6, *B* and *C*. Further exemplified by co-immunoprecipitation studies, hyperhomocysteinemic mice displayed robust amounts of TXNIP protein pulled down together with NLRP3 compared with ND fed mice, suggesting that NLRP3-TXNIP binding was enhanced during hHcys (Fig. 6*D*). However, this enhanced NLRP3-TXNIP binding was not observed in glomeruli of TXNIP shRNA-transfected or verapamil-treated mice. These NLRP3 inflammasome-inhibiting effects were not due to reductions in plasma Hcys concentration from TXNIP shRNA transfection or verapamil administration (Fig. 6*E*).

Inhibition of TXNIP Blocked Renal Caspase-1 Activation and IL-1β Secretion Induced by hHcys—Caspase-1 activity and IL-1β production was measured to evaluate the effects of *in vivo*

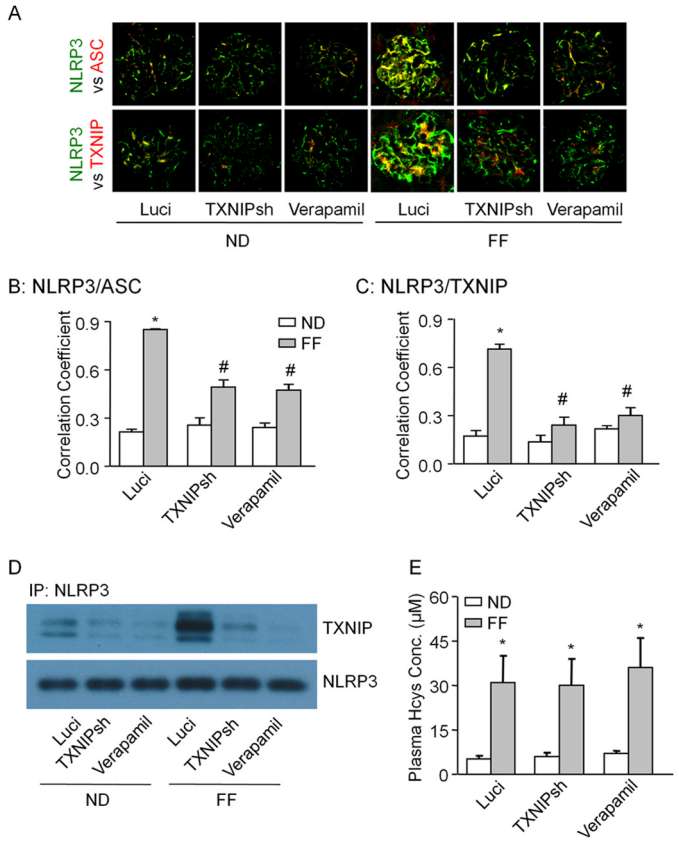

FIGURE 6. ***In vivo* inhibition of TXNIP and its effect on NLRP3 inflammasome formation.** *A*, confocal microscopy demonstrated the colocalization between NLRP3 (*green*) with ASC (*red*) and NLRP3 (*green*) with TXNIP (*red*) in the glomeruli of luciferase (*Luci*), TXNIP shRNA (*TXNIPsh*), and verapamil-treated mice maintained on either a ND or FF diet. *B* and *C*, summarized data showing the quantification of the extent of colocalization between NLRP3 with ASC and NLRP3 with TXNIP ($n = 6$). *D*, co-immunoprecipitation studies demonstrated robust *in vivo* TXNIP-NLRP3 binding in mice with hHcys, which was not evident after TXNIP inhibition ($n = 5$). *E*, plasma Hcys concentrations (*Conc.*) of all mice fed a FF diet were all elevated and were unaffected by *in vivo* TXNIP inhibition either by shRNA transfection or verapamil administration ($n = 4–6$). *, $p < 0.05$ *versus* luciferase ND; #, $p < 0.05$ *versus* luciferase FF.

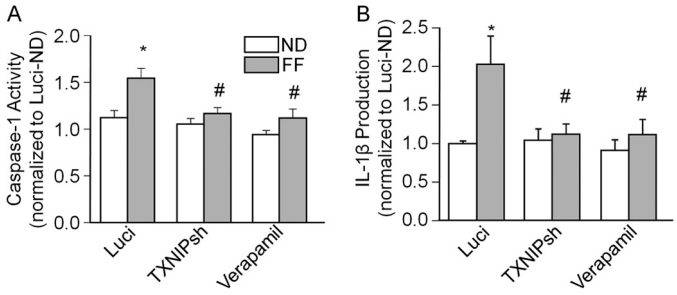

FIGURE 7. ***In vivo* TXNIP shRNA transfection and verapamil treatment blocked caspase-1 activation and IL-1β production.** *A*, caspase-1 activity, shown as fold change *versus* luciferase ND, in luciferase, TXNIP shRNA, and verapamil-treated mice with FF diet-induced hHcys ($n = 5–6$). *B*, *in vivo* TXNIP inhibition prevented hHcys-induced IL-1β production ($n = 6$). *Luci*, luciferase; *TXNIPsh*, TXNIP shRNA. *, $p < 0.05$ *versus* luciferase ND; #, $p < 0.05$ *versus* luciferase FF.

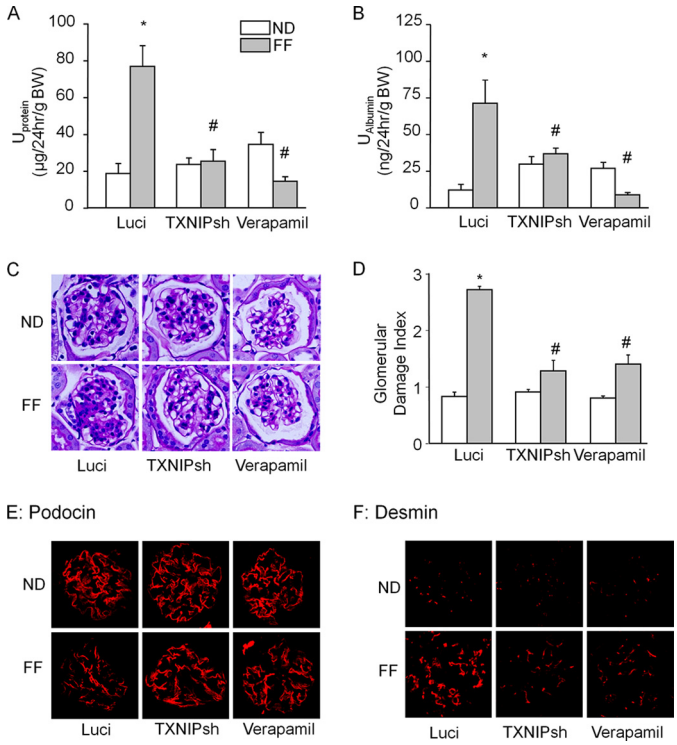

FIGURE 8. **Amelioration of hHcys-induced glomerular damage by *in vivo* TXNIP inhibition.** *A* and *B*, hHcys-induced increases in proteinuria and albuminuria were diminished by TXNIP shRNA transfection and verapamil administration ($n = 6–8$). *C*, observation of glomerular morphology in periodic acid-Schiff-stained slides revealed severe pathological changes in the glomeruli of luciferase FF mice, which were prevented in TXNIP inhibited mice. *D*, pathological changes in the glomeruli were semiquantitatively scored and summarized as the glomerular damage index ($n = 5$). *E* and *F*, *in vivo* immunofluorescent staining of podocin and desmin to assess glomerular podocyte condition ($n = 6$). *BW*, body weight; *Luci*, luciferase; *TXNIPsh*, TXNIP shRNA. *, $p < 0.05$ *versus* luciferase ND; #, $p < 0.05$ *versus* luciferase FF.

TXNIP inhibition on hHcys-induced NLRP3 inflammasome activation (Fig. 7, *A* and *B*). Mice with hHcys induced by the FF diet displayed increased caspase-1 activation and IL-1β production compared with those on the ND, suggesting increased NLRP3 inflammasome activity in the cortical tissue. This activation was not apparent in the mice where TXNIP was inhibited by either shRNA transfection or verapamil treatment.

hHcys-induced Glomerular Dysfunction Was Attenuated by TXNIP Inhibition—This study, as well as many of our previous studies, clearly demonstrated the ability of our hyperhomocysteinemic mouse model to induce significant glomerular dysfunction and ultimate sclerosis (12, 26, 32). Demonstrated in Fig. 8, luciferase-transfected mice on the FF diet exhibited severe urinary protein and albumin excretion compared with control mice on the ND. Furthermore, mice with hHcys displayed aberrant glomerular morphology, characterized by a shrunken phenotype with extracellular matrix and collagen deposition, capillary collapse, and mesangial cell expansion (Fig. 8*C*). Decreased expression of podocyte-specific marker, podocin, and increase in podocyte damage marker, desmin, both hallmarks of podocyte injury, was also observed in the glomeruli of mice on the FF diet (Fig. 8, *E* and *F*). *In vivo* TXNIP inhibition by shRNA transfection or verapamil treatment was able to prevent all of the aforementioned destructive changes induced by hHcys as shown by the reduction of proteinuria, albuminuria, glomerular pathological changes, and restored expression of podocin and desmin. These data provided solid evidence that TXNIP plays a detrimental role in hHcys-induced podocyte and glomerular damage, which is due to its ability to mediate NLRP3 inflammasome activation.

DISCUSSION

The present study was designed to explore the role of TXNIP in hHcys-induced NLRP3 inflammasome activation and associated podocyte injury and glomerular sclerosis. It was found that Hcys treatment of podocytes up-regulated protein expression of TXNIP, which resulted in increased binding of TXNIP with inflammasome protein NLRP3. Both *in vitro* and *in vivo* inhibition of TXNIP by its inhibitor verapamil or RNA interference blocked TXNIP expression and prevented TXNIP-NLRP3 binding and subsequent NLRP3 inflammasome activation in response to Hcys. These findings demonstrate the critical role of TXNIP binding in the activation of NLRP3 inflammasomes and subsequent podocyte injury and glomerular dysfunction or sclerosis.

The activation of NLRP3 inflammasomes has been implicated in a growing number of diverse pathological conditions, ranging from bacterial infections to cardiovascular dysfunction and metabolic syndrome (33–36). ROS produced by many known activators of NLRP3 inflammasomes are critical for triggering NLRP3 inflammasome formation and activation (37). Despite studies that have demonstrated an important role for ROS in inflammasome activation, it remains unclear how NLRP3 is able to sense redox changes in a variety of cells, in particular, in podocytes during hHcys. Through a yeast two-hybrid screen, it has been shown that TXNIP, a ROS sensor and an endogenous inhibitor of the antioxidant thioredoxin, is a binding partner of NLRP3. TXNIP, also known as VDUP-1 (vitamin D3 up-regulated protein 1) and TBP-2 (thioredoxin-binding protein-2), plays a critical role in growth suppression, making it particularly important in tumor and cancer progression by causing G1 cell cycle arrest. It is also a crucial regulator of lipid metabolism where overexpression of TXNIP during hyperglycemia, causing β-cell death and impaired insulin secretion (38). Zhou *et al.* (14) confirmed an important role for TXNIP in the pathogenesis of type 2 diabetes by showing that TXNIP binding to NLRP3 was essential for ROS-mediated inflammasome activation. Additionally, in human and rat kidneys, TXNIP mRNA and protein is most abundantly expressed in the glomeruli (39), and although some studies have demonstrated its up-regulation in response to high glucose (40, 41), there have been no studies to date exploring the effects of Hcys on TXNIP, in particular, in podocyte or glomerular injury. In the current study, we sought to determine the effects of Hcys on TXNIP and whether its binding to NLRP3 mediates inflammasome activation in hHcys-induced podocyte and glomerular injury.

Using genetic manipulations and pharmacologic inhibitors of TXNIP, we found that TXNIP mRNA and protein expression was significantly reduced after transfection of siRNA into cultured mouse podocytes (data not shown) and local transfection of TXNIP shRNA *in vivo* into mouse kidneys (Fig. 5, *C* and *D*). To complement this genetic manipulation, we used pharmacologic calcium channel blocker verapamil to inhibit TXNIP expression both *in vitro* and *in vivo*. It has been demonstrated that verapamil, when administered to mice through the drinking water at an average dose of 100 mg/kg/day, decreased diabetes-induced cardiomyocyte apoptosis, an effect specifically due its potent inhibition of TXNIP expression (19). Additionally, verapamil enhanced β-cell survival and function through its reduction of β-cell TXNIP expression (42), and this may be due to verapamil-induced transcriptional repression of TXNIP (43). In the present study, verapamil, at a dose of 50 μM, strongly inhibited TXNIP expression in podocytes (data not shown), inhibited TXNIP binding to NLRP3, and prevented Hcys-induced NLRP3 inflammasome formation and activation in podocytes. *In vivo* experiments furthermore displayed TXNIP inhibition hindering caspase-1 activation and IL-1β maturation in hyperhomocysteinemic mice (Fig. 7). To our knowledge, this is the first evidence showing the critical role of TXNIP-NLRP3 binding in mediating podocyte inflammasome activation in response to Hcys stimulation.

Elevated levels of Hcys has been recognized as a pathogenic risk factor for many sclerotic diseases, ranging from cardiovascular to neurological diseases, as well as our particular interest, glomerular sclerosis and end stage renal disease. We and others (8, 44, 45) have provided evidence that prolonged elevation of blood homocysteine level results in hallmarks typical of glomerular sclerosis, including glomerular hypercellularity, capillary collapse, and fibrous extracellular matrix deposition. The current study demonstrated that hHcys produced many of these same characteristic features of podocyte and glomerular injury. Hcys-induced podocyte dysfunction both *in vitro* and *in vivo* was exhibited through down-regulation of podocin and up-regulation of damage marker desmin, as well as in the increased proteinuria, albuminuria, and sclerotic morphological changes in hyperhomocysteinemic mice (Figs. 4 and 8). However, inhibition of TXNIP by either genetic manipulation or by verapamil treatment prevented the Hcys-induced detrimental effects on both podocytes in culture and glomerular structure and function. Verapamil has long been demonstrated to have glomerular protective effects (46, 47); however, our study is the first to demonstrate that, at least in hHcys-induced glomerular injury, this protective effect of verapamil is associated with its inhibitory action of TXNIP.

In other studies, inhibition of TXNIP expression by verapamil has also been reported (48), but this effect has been extended to other calcium channel blockers and inhibitors such as diltiazem and $NiCl_2$, as well as with calcium chelator EGTA. This suggests that this inhibition of TXNIP function is perhaps not a direct effect of verapamil itself, but more likely due to a reduction in intracellular calcium concentrations (42). Additionally, calcium signaling is emerging as an important component of NLRP3 inflammasome activation. Brough *et al.* (49) first demonstrated such role of calcium signaling when they found suppressed IL-1β maturation following pretreatment of cells with a calcium chelator, BAPTA-AM. This process may involve ER stress, calcium release from ER, and TXNIP binding (49–51). Although these possible nonspecific effects may not be excluded, our multifaceted approach of genetic and pharmacologic interventions give us confidence that the diminished NLRP3 inflammasome activation by verapamil is indeed due to the reduction in TXNIP expression and binding. It should be noted that the contribution of various calcium signaling pathways in the mediation or regulation of NLRP3 inflammasome

activation in podocytes or other cells indeed warrants future exploration.

Taken together, we provided direct evidence that inhibition of TXNIP and diminished TXNIP-NLRP3 binding reduced NLRP3 inflammasome formation and activation, even in the continued presence of elevated Hcys or during hHcys in mice. This reduction in TXNIP-mediated inflammasome activation protected podocytes from the early deleterious effects of Hcys that, if left unattended, may ultimately progress to glomerular sclerosis and potential end stage renal disease. This study revealed TXNIP inhibition as a new protective mechanism of verapamil and has immense clinical implications in preventing podocyte and glomerular injury related to hHcys. These findings elucidate a novel molecular mechanism mediating the activation of inflammasomes in podocytes upon Hcys, which may uncover new potential therapeutic targets for the treatment and prevention of end stage renal disease during hHcys.

REFERENCES

1. Bakker, P. J., Butter, L. M., Kors, L., Teske, G. J., Aten, J., Sutterwala, F. S., Florquin, S., and Leemans, J. C. (2014) Nlrp3 is a key modulator of diet-induced nephropathy and renal cholesterol accumulation. *Kidney Int.* **85,** 1112–1122
2. Yin, Y., Pastrana, J. L., Li, X., Huang, X., Mallilankaraman, K., Choi, E. T., Madesh, M., Wang, H., and Yang, X. F. (2013) Inflammasomes: sensors of metabolic stresses for vascular inflammation. *Front. Biosci.* **18,** 638–649
3. Pétrilli, V., and Martinon, F. (2007) The inflammasome, autoinflammatory diseases, and gout. *Joint Bone Spine* **74,** 571–576
4. Martinon, F., Agostini, L., Meylan, E., and Tschopp, J. (2004) Identification of bacterial muramyl dipeptide as activator of the NALP3/cryopyrin inflammasome. *Curr. Biol.* **14,** 1929–1934
5. O'Connor, W., Jr., Harton, J. A., Zhu, X., Linhoff, M. W., and Ting, J. P. (2003) Cutting edge: CIAS1/cryopyrin/PYPAF1/NALP3/CATERPILLER 1.1 is an inducible inflammatory mediator with NF-κB suppressive properties. *J. Immunol.* **171,** 6329–6333
6. Martinon, F., and Tschopp, J. (2005) NLRs join TLRs as innate sensors of pathogens. *Trends Immunol.* **26,** 447–454
7. Yang, F., Wang, Z., Wei, X., Han, H., Meng, X., Zhang, Y., Shi, W., Li, F., Xin, T., Pang, Q., and Yi, F. (2014) NLRP3 deficiency ameliorates neurovascular damage in experimental ischemic stroke. *J. Cereb. Blood Flow Metab.* **34,** 660–667
8. Li, N., Chen, Y. F., and Zou, A. P. (2002) Implications of hyperhomocysteinemia in glomerular sclerosis in hypertension. *Hypertension* **39,** 443–448
9. Kalani, A., Kamat, P. K., Givvimani, S., Brown, K., Metreveli, N., Tyagi, S. C., and Tyagi, N. (2014) Nutri-epigenetics ameliorates blood-brain barrier damage and neurodegeneration in hyperhomocysteinemia: role of folic acid. *J. Mol. Neurosci.* **52,** 202–215
10. Nilsson, K., Gustafson, L., and Hultberg, B. (2007) Plasma homocysteine is elevated in elderly patients with memory complaints and vascular disease. *Dement. Geriatr. Cogn. Disord.* **23,** 321–326
11. Zhang, C., Boini, K. M., Xia, M., Abais, J. M., Li, X., Liu, Q., and Li, P. L. (2012) Activation of Nod-like receptor protein 3 inflammasomes turns on podocyte injury and glomerular sclerosis in hyperhomocysteinemia. *Hypertension* **60,** 154–162
12. Abais, J. M., Zhang, C., Xia, M., Liu, Q., Gehr, T. W., Boini, K. M., and Li, P. L. (2013) NADPH oxidase-mediated triggering of inflammasome activation in mouse podocytes and glomeruli during hyperhomocysteinemia. *Antioxid. Redox. Signal* **18,** 1537–1548
13. Abais, J. M., Xia, M., Li, G., Gehr, T. W., Boini, K. M., and Li, P. L. (2014) Contribution of endogenously produced reactive oxygen species to the activation of podocyte NLRP3 inflammasomes in hyperhomocysteinemia. *Free Radic. Biol. Med.* **67,** 211–220
14. Zhou, R., Tardivel, A., Thorens, B., Choi, I., and Tschopp, J. (2010) Thioredoxin-interacting protein links oxidative stress to inflammasome activation. *Nat. Immunol.* **11,** 136–140
15. Schwartz, E. J., Cara, A., Snoeck, H., Ross, M. D., Sunamoto, M., Reiser, J., Mundel, P., and Klotman, P. E. (2001) Human immunodeficiency virus-1 induces loss of contact inhibition in podocytes. *J. Am. Soc. Nephrol.* **12,** 1677–1684
16. Mundel, P., Reiser, J., Zúñiga Mejía Borja, A., Pavenstädt, H., Davidson, G. R., Kriz, W., and Zeller, R. (1997) Rearrangements of the cytoskeleton and cell contacts induce process formation during differentiation of conditionally immortalized mouse podocyte cell lines. *Exp. Cell Res.* **236,** 248–258
17. Yi, F., Zhang, A. Y., Li, N., Muh, R. W., Fillet, M., Renert, A. F., and Li, P. L. (2006) Inhibition of ceramide-redox signaling pathway blocks glomerular injury in hyperhomocysteinemic rats. *Kidney Int.* **70,** 88–96
18. Joles, J. A., Kunter, U., Janssen, U., Kriz, W., Rabelink, T. J., Koomans, H. A., and Floege, J. (2000) Early mechanisms of renal injury in hypercholesterolemic or hypertriglyceridemic rats. *J. Am. Soc. Nephrol.* **11,** 669–683
19. Chen, J., Cha-Molstad, H., Szabo, A., and Shalev, A. (2009) Diabetes induces and calcium channel blockers prevent cardiac expression of proapoptotic thioredoxin-interacting protein. *Am. J. Physiol. Endocrinol. Metab.* **296,** E1133–1139
20. Zhang, C., Xia, M., Boini, K. M., Li, C. X., Abais, J. M., Li, X. X., Laperle, L. A., and Li, P. L. (2011) Epithelial-to-mesenchymal transition in podocytes mediated by activation of NADPH oxidase in hyperhomocysteinemia. *Pflugers Arch.* **462,** 455–467
21. Raij, L., Azar, S., and Keane, W. (1984) Mesangial immune injury, hypertension, and progressive glomerular damage in Dahl rats. *Kidney Int.* **26,** 137–143
22. Xiong, J., Xia, M., Xu, M., Zhang, Y., Abais, J. M., Li, G., Riebling, C. R., Ritter, J. K., Boini, K. M., and Li, P. L. (2013) Autophagy maturation associated with CD38-mediated regulation of lysosome function in mouse glomerular podocytes. *J. Cell. Mol. Med.* **17,** 1598–1607
23. Zhang, A. Y., Yi, F., Teggatz, E. G., Zou, A. P., and Li, P. L. (2004) Enhanced production and action of cyclic ADP-ribose during oxidative stress in small bovine coronary arterial smooth muscle. *Microvasc. Res.* **67,** 159–167
24. Grynkiewicz, G., Poenie, M., and Tsien, R. Y. (1985) A new generation of Ca^{2+} indicators with greatly improved fluorescence properties. *J. Biol. Chem.* **260,** 3440–3450
25. Zhang, C., Hu, J. J., Xia, M., Boini, K. M., Brimson, C., and Li, P. L. (2010) Redox signaling via lipid raft clustering in homocysteine-induced injury of podocytes. *Biochim. Biophys. Acta* **1803,** 482–491
26. Boini, K. M., Xia, M., Li, C., Zhang, C., Payne, L. P., Abais, J. M., Poklis, J. L., Hylemon, P. B., and Li, P. L. (2011) Acid sphingomyelinase gene deficiency ameliorates the hyperhomocysteinemia-induced glomerular injury in mice. *Am. J. Pathol.* **179,** 2210–2219
27. Srinivasula, S. M., Poyet, J. L., Razmara, M., Datta, P., Zhang, Z., and Alnemri, E. S. (2002) The PYRIN-CARD protein ASC is an activating adaptor for caspase-1. *J. Biol. Chem.* **277,** 21119–21122
28. Kawachi, H., Miyauchi, N., Suzuki, K., Han, G. D., Orikasa, M., and Shimizu, F. (2006) Role of podocyte slit diaphragm as a filtration barrier. *Nephrology* **11,** 274–281
29. Floege, J., Alpers, C. E., Sage, E. H., Pritzl, P., Gordon, K., Johnson, R. J., and Couser, W. G. (1992) Markers of complement-dependent and complement-independent glomerular visceral epithelial cell injury *in vivo*. Expression of antiadhesive proteins and cytoskeletal changes. *Lab. Invest.* **67,** 486–497
30. Kang, D. H., and Johnson, R. J. (2003) Vascular endothelial growth factor: a new player in the pathogenesis of renal fibrosis. *Curr. Opin. Nephrol. Hypertens.* **12,** 43–49
31. Boini, K. M., Xia, M., Abais, J. M., Li, G., Pitzer, A. L., Gehr, T. W., Zhang, Y., and Li, P. L. (2014) Activation of inflammasomes in podocyte injury of mice on the high fat diet: effects of ASC gene deletion and silencing. *Biochim. Biophys. Acta* **1843,** 836–845
32. Zhang, C., Hu, J. J., Xia, M., Boini, K. M., Brimson, C. A., Laperle, L. A., and Li, P. L. (2010) Protection of podocytes from hyperhomocysteinemia-induced injury by deletion of the gp91phox gene. *Free Radic Biol. Med.* **48,** 1109–1117

33. Benko, S., Philpott, D. J., and Girardin, S. E. (2008) The microbial and danger signals that activate Nod-like receptors. *Cytokine* **43,** 368–373
34. Duewell, P., Kono, H., Rayner, K. J., Sirois, C. M., Vladimer, G., Bauernfeind, F. G., Abela, G. S., Franchi, L., Nuñez, G., Schnurr, M., Espevik, T., Lien, E., Fitzgerald, K. A., Rock, K. L., Moore, K. J., Wright, S. D., Hornung, V., and Latz, E. (2010) NLRP3 inflammasomes are required for atherogenesis and activated by cholesterol crystals. *Nature* **464,** 1357–1361
35. Overley-Adamson, B., Artlett, C. M., Stephens, C., Sassi-Gaha, S., Weis, R. D., and Thacker, J. D. (2014) Targeting the unfolded protein response, XBP1, and the NLRP3 inflammasome in fibrosis and cancer. *Cancer Biol. Ther.* **15, 452–462**
36. Henao-Mejia, J., Elinav, E., Jin, C., Hao, L., Mehal, W. Z., Strowig, T., Thaiss, C. A., Kau, A. L., Eisenbarth, S. C., Jurczak, M. J., Camporez, J. P., Shulman, G. I., Gordon, J. I., Hoffman, H. M., and Flavell, R. A. (2012) Inflammasome-mediated dysbiosis regulates progression of NAFLD and obesity. *Nature* **482,** 179–185
37. Tschopp, J., and Schroder, K. (2010) NLRP3 inflammasome activation: The convergence of multiple signalling pathways on ROS production? *Nat. Rev. Immunol.* **10,** 210–215
38. Minn, A. H., Pise-Masison, C. A., Radonovich, M., Brady, J. N., Wang, P., Kendziorski, C., and Shalev, A. (2005) Gene expression profiling in INS-1 cells overexpressing thioredoxin-interacting protein. *Biochem. Biophys. Res. Commun.* **336,** 770–778
39. Advani, A., Gilbert, R. E., Thai, K., Gow, R. M., Langham, R. G., Cox, A. J., Connelly, K. A., Zhang, Y., Herzenberg, A. M., Christensen, P. K., Pollock, C. A., Qi, W., Tan, S. M., Parving, H. H., and Kelly, D. J. (2009) Expression, localization, and function of the thioredoxin system in diabetic nephropathy. *J. Am. Soc. Nephrol.* **20,** 730–741
40. Shah, A., Xia, L., Goldberg, H., Lee, K. W., Quaggin, S. E., and Fantus, I. G. (2013) Thioredoxin-interacting protein mediates high glucose-induced reactive oxygen species generation by mitochondria and the NADPH oxidase, Nox4, in mesangial cells. *J. Biol. Chem.* **288,** 6835–6848
41. Li, X., Rong, Y., Zhang, M., Wang, X. L., LeMaire, S. A., Coselli, J. S., Zhang, Y., and Shen, Y. H. (2009) Up-regulation of thioredoxin interacting protein (Txnip) by p38 MAPK and FOXO1 contributes to the impaired thioredoxin activity and increased ROS in glucose-treated endothelial cells. *Biochem. Biophys. Res. Commun.* **381,** 660–665
42. Xu, G., Chen, J., Jing, G., and Shalev, A. (2012) Preventing β-cell loss and diabetes with calcium channel blockers. *Diabetes* **61,** 848–856
43. Cha-Molstad, H., Xu, G., Chen, J., Jing, G., Young, M. E., Chatham, J. C., and Shalev, A. (2012) Calcium channel blockers act through nuclear factor Y to control transcription of key cardiac genes. *Mol. Pharmacol.* **82,** 541–549
44. Cao, L., Lou, X., Zou, Z., Mou, N., Wu, W., Huang, X., and Tan, H. (2013) Folic acid attenuates hyperhomocysteinemia-induced glomerular damage in rats. *Microvasc. Res.* **89,** 146–152
45. Sen, U., Munjal, C., Qipshidze, N., Abe, O., Gargoum, R., and Tyagi, S. C. (2010) Hydrogen sulfide regulates homocysteine-mediated glomerulosclerosis. *Am. J. Nephrol.* **31,** 442–455
46. Harris, D. C., Hammond, W. S., Burke, T. J., and Schrier, R. W. (1987) Verapamil protects against progression of experimental chronic renal failure. *Kidney Int.* **31,** 41–46
47. Pelayo, J. C., Harris, D. C., Shanley, P. F., Miller, G. J., and Schrier, R. W. (1988) Glomerular hemodynamic adaptations in remnant nephrons: effects of verapamil. *Am. J. Physiol.* **254,** F425–431
48. Al-Gayyar, M. M., Abdelsaid, M. A., Matragoon, S., Pillai, B. A., and El-Remessy, A. B. (2011) Thioredoxin interacting protein is a novel mediator of retinal inflammation and neurotoxicity. *Br. J. Pharmacol.* **164,** 170–180
49. Brough, D., Le Feuvre, R. A., Wheeler, R. D., Solovyova, N., Hilfiker, S., Rothwell, N. J., and Verkhratsky, A. (2003) Ca^{2+} stores and Ca^{2+} entry differentially contribute to the release of IL-1 β and IL-1 α from murine macrophages. *J. Immunol.* **170,** 3029–3036
50. Oslowski, C. M., Hara, T., O'Sullivan-Murphy, B., Kanekura, K., Lu, S., Hara, M., Ishigaki, S., Zhu, L. J., Hayashi, E., Hui, S. T., Greiner, D., Kaufman, R. J., Bortell, R., and Urano, F. (2012) Thioredoxin-interacting protein mediates ER stress-induced β cell death through initiation of the inflammasome. *Cell Metab.* **16,** 265–273
51. Lerner, A. G., Upton, J. P., Praveen, P. V., Ghosh, R., Nakagawa, Y., Igbaria, A., Shen, S., Nguyen, V., Backes, B. J., Heiman, M., Heintz, N., Greengard, P., Hui, S., Tang, Q., Trusina, A., Oakes, S. A., and Papa, F. R. (2012) IRE1alpha induces thioredoxin-interacting protein to activate the NLRP3 inflammasome and promote programmed cell death under irremediable ER stress. *Cell Metab.* **16,** 250–264